Christopher A. G. Kalnins, Heike Ebendorff-Heidepriem, Nigel A. Spooner and Tanya M. Monro

Enhanced radiation dosimetry of fluoride phosphate glass optical fibres by terbium (III) doping

Optical Materials Express, 2016; 6(12):3692-3703

Published version http://dx.doi.org/10.1364/OME.6.003692

Research Article | Vol. 6, No. 12 | 1 Dec 2016 | OPTICAL MATERIALS EXPRESS 3692

Optical Materials EXPRESS

Enhanced radiation dosimetry of fluoride phosphate glass optical fibres by terbium (III) doping

CHRISTOPHER A. G. KALNINS,[1,2,*] HEIKE EBENDORFF-HEIDEPRIEM,[1,2] NIGEL A. SPOONER[1,2,3] AND TANYA M. MONRO[1,4]

[1] *Institute for Photonics and Advanced Sensing and School of Physical Sciences, University of Adelaide, Adelaide 5005, Australia*
[2] *ARC Research Hub for Australian Copper-Uranium, Australia*
[3] *Defence Science & Technology Group, Edinburgh 5111, SA, Australia*
[4] *University of South Australia, Adelaide, SA 5001, Australia*
[*] *chris.kalnins@adelaide.edu.au*

Abstract: Fluoride phosphate (FP) glass fibres have been developed for radiation dosimetry based on the mechanism of optically stimulated luminescence (OSL). Doping with Tb^{3+} ions improved the materials sensitivity; for samples melted in oxidising conditions, OSL intensity was increased from 8.8×10^5 cnts/g/Gy for undoped glass to 812.3×10^5 cnts/g/Gy for Tb^{3+}-doped glass. The radiation sensor performance of Tb^{3+}-doped glass fibres under both beta and X-ray irradiation demonstrated the capability of the fibres for radiation dosimetry applications.

OCIS codes: (060.2370) Fiber optics sensors; (160.2540) Fluorescent and luminescent materials; (160.2750) Glass and other amorphous materials; (160.5690) Rare-earth-doped materials; (260.3800) Luminescence; (350.5610) Radiation.

References and links

1. A. L. Huston, B. L. Justus, P. L. Falkenstein, R. W. Miller, H. Ning, and R. Altemus, "Optically stimulated luminescent glass optical fibre dosemeter," Radiat. Prot. Dosim. **101**, 23–26 (2002).
2. A. M. C. Santos, M. Mohammadi, and S. Afshar, "Investigation of a fibre-coupled beryllium oxide (BeO) ceramic luminescence dosimetry system," Radiat. Meas. **70**, 52–58 (2014).
3. J. C. Polf, S. W. S. McKeever, M. S. Akselrod, and S. Holmstrom, "A real-time, fibre optic dosimetry system using Al_2O_3:C fibres," Radiat. Prot. Dosim. **100**, 301–304 (2002).
4. G. Ranchoux, S. Magne, J. P. Bouvet, and P. Ferdinand, "Fibre remote optoelectronic gamma dosimetry based on optically stimulated luminescence of Al_2O_3:C," Radiat. Prot. Dosim. **100**, 255–260 (2002).
5. J. C. Polf, E. G. Yukihara, M. S. Akselrod, and S. W. S. McKeever, "Real-time luminescence from Al_2O_3:C fiber dosimeters," Radiat. Meas. **38**, 227–240 (2004).
6. M. C. Aznar, C. E. Andersen, L. Bøtter-Jensen, S. A. J. Back, S. Mattsson, F. Kjær-Kristoffersen, and J. Medin, "Real-time optical-fibre luminescence dosimetry for radiotherapy: physical characteristics and applications in photon beams," Phys. Med. Biol. **49**, 1655–1669 (2004).
7. J. M. Edmund, C. E. Andersen, C. J. Marckmann, M. C. Aznar, M. S. Akselrod, and L. Bøtter-Jensen, "CW-OSL measurement protocols using optical fibre Al_2O_3:C," Radiat. Prot. Dosim. **119**, 368 (2006).
8. C. E. Andersen, J. M. Edmund, and S. M. S. Damkjær, "Precision of RL/OSL medical dosimetry with fiber-coupled Al_2O_3:C: Influence of readout delay and temperature variations," Radiat. Meas. **45**, 653–657 (2010).
9. C. E. Andersen, S. M. S. Damkjær, G. Kertzscher, S. Greilich, and M. C. Aznar, "Fiber-coupled radioluminescence dosimetry with saturated Al_2O_3:C crystals: Characterization in 6 and 18 MV photon beams," Radiat. Meas. **46**, 1090–1098 (2011).
10. C. A. G. Kalnins, H. Ebendorff-Heidepriem, N. A. Spooner, and T. M. Monro, "Optically stimulated luminescence in fluoride–phosphate glass for radiation dosimetry," J. Am. Ceram. Soc. **94**, 474 – 477 (2011).
11. C. A. G. Kalnins, H. Ebendorff-Heidepriem, N. A. Spooner, and T. M. Monro, "Radiation dosimetry using optically stimulated luminescence in fluoride phosphate optical fibres," Opt. Mater. Express **2**, 62 – 70 (2012).
12. D. He, C. Yu, S. Li, and L. Hu, "Effect of Tb^{3+} concentration and sensitization of Ce^{3+} on luminescence properties of terbium doped phosphate scintillating glass," J. Alloy. Compd. **509**, 1906–1909 (2011).
13. S. Huang and M. Gu, "Enhanced luminescent properties of Tb^{3+} ions in transparent glass ceramics containing $BaGdF_5$ nanocrystals," J. Non-Cryst. Solids **358**, 77–80 (2012).
14. Y. Zhang, J. Lv, N. Ding, S. Jiang, T. Zheng, and J. Li, "Tunable luminescence and energy transfer from Gd^{3+} to Tb^{3+} ions in silicate oxyfluoride scintillating glasses via varying Tb^{3+} concentration," J. Non-Cryst. Solids **423**,

#274134 http://dx.doi.org/10.1364/OME.6.003692
Journal © 2016 Received 19 Aug 2016; revised 22 Oct 2016; accepted 23 Oct 2016; published 1 Nov 2016

Optical Materials EXPRESS

30–34 (2015).
15. Y. Yao, L. Liu, Y. Zhang, D. Chen, Y. Fang, and G. Zhao, "Optical properties of Ce^{3+} doped fluorophosphates scintillation glasses," Opt. Mater. **51**, 94–97 (2016).
16. G. Vedda, A. Chiodini, N. D. Martino, D. Fasoli, M. Keffer, S. L. A. Martnini, M. Moretti, F. Spinolo, G. Nikl, M. Solovieva, and N. Brambilla, "Ce^{3+}-doped fibers for remote radiation dosimetry," Appl. Phys. Lett. **85**, 6356–6358 (2004).
17. W. Chewpraditkul, Y. Shen, D. Chen, B. Yu, P. Prusa, M. Nikl, A. Beitlerova, and C. Wanarak, "Luminescence and scintillation of Ce^{3+}-doped high silica glass," Opt. Mater. **34**, 1762–1766 (2012).
18. W. Chewpraditkul, Y. Shen, D. Chen, M. Nikl, and A. Beitlerova, "Luminescence of Ce^{3+}- and Eu^{2+}- doped silica glasses under UV and X-ray excitation," J. Optoelectron. Adv. Mater. **15**, 94–98 (2013).
19. S. Liu, S. Zheng, C. Tang, X. Li, W. Xu, Q. Sheng, and D. Chen, "Photoluminescence and radioluminescence properties of Yb^{2+}-doped silica glass," Mater. Lett. **144**, 43–45 (2015).
20. I. Veronese, C. D. Mattia, M. Fasoli, N. Chiodini, M. C. Cantone, F. Moretti, C. Dujardin, and A. Vedda, "Role of optical fiber drawing in radioluminescence hysteresis of Yb-doped silica," J. Phys. Chem. C **119**, 15572–15578 (2015).
21. W. Chewpraditkul, Y. Shen, D. Chen, A. Beitlerova, and M. Nikl, "Luminescence of Tb^{3+}-doped high silica glass under UV and X-ray excitation," Opt. Mater. **35**, 426–430 (2013).
22. H. Ebendorff-Heidepriem and D. Ehrt, "Spectroscopic properties of Eu^{3+} and Tb^{3+} ions for local structure investigations of fluoride phosphate and phosphate glasses," J. Non-Cryst. Solids **208**, 205–216 (1996).
23. H. Ebendorff-Heidepriem and D. Ehrt, "Formation and UV absorption of cerium, europium and terbium ions in different valencies in glasses," Opt. Mater. **15**, 7–25 (2000).
24. C. A. G. Kalnins, N. A. Spooner, T. M. Monro, and H. Ebendorff-Heidepriem, "Surface analysis and treatment of extruded fluoride phosphate glass preforms for optical fibre fabrication," J. Am. Ceram. Soc. **99**, 1874–1877 (2016).
25. M. J. Chen, Y. M. Stokes, P. Buchak, D. G. Crowdy, H. T. Foo, A. Dowler, and H. Ebendorff-Heidepriem, "Drawing tubular fibres: Experiments versus mathematical modelling," Opt. Mater. Express **6**, 166–180 (2016).
26. Schott Glass Company, "Optical Glass Data Sheets" http://www.schott.com/advanced_optics/english/download/.
27. J. Hecht, *Understanding Fiber Optics* (Pearson Prentice Hall, 2006).
28. H. Ebendorff-Heidepriem and D. Ehrt, "Relationships between glass structure and spectroscopic properties of Eu^{3+} and Tb^{3+} doped glasses," Ber. Bunsenges. Phys. Chem. **100**, 1621–1624 (1996).
29. D. Ehrt, "Redox behavior of polyvalent ions in the ppm range," J. Non-Cryst. Solids **196**, 304–308 (1996).
30. N. Duhamel-Henry, J. L. Adam, B. Jacquier, and C. Linarès, "Photoluminescence of new fluorophosphate glasses containing a high concentration of terbium (III) ions," Opt. Mater. **5**, 197–207 (1996).
31. C. A. G. Kalnins, N. A. Spooner, H. Ebendorff-Heidepriem, and T. M. Monro, "Luminescent properties of fluoride phosphate glass for radiation dosimetry," Opt. Mater. Express **3**, 960–967 (2013).
32. J. R. Prescott, P. J. Fox, R. A. Akber, and H. E. Jensen, "Thermoluminescence emission spectrometer," Appl. Opt. **27**, 3496–3502 (1988).
33. S. W. S. McKeever, *Thermoluminescence of Solids* (Cambridge University, 1985).
34. R. Chen and S. W. S. McKeever, *Theory of Thermoluminescence and Related Phenomena* (World Scientific, 1997).
35. C. Furetta and P. Weng, *Operational Thermoluminescence Dosimetry* (World Scientific, 1998).
36. H. Ebendorff-Heidepriem and D. Ehrt, "UV radiation effects in fluoride phosphate glasses," J. Non-Cryst. Solids **196**, 113–117 (1996).
37. X. Zou and H. Toratani, "Radiation resistance of fluorophosphate glasses for high performance optical fiber in the ultraviolet region," J. Appl. Phys. **81**, 3354–3362 (1997).

1. Introduction

Optical fibre dosimetry has been studied extensively due to the usefulness of fibres as probes and distributed sensing devices, applications include medicine and monitoring applications. Various methods have been demonstrated, using mainly radioluminescence, photodarkening and optically stimulated luminescence (OSL). Both intrinsic and extrinsic sensing methods have been used. Intrinsic sensing is defined as occurring when the optical fibre itself is the radiation sensing component, while extrinsic is defined as where an optical fibre is coupled to a phosphor crystal for the purposes of transmitting an optical signal to the detector.

The use of optically stimulated luminescence as the sensing mechanism has mostly been demonstrated using an extrinsic, chip-coupled design. Cu^{+}-doped silica glass [1], BeO [2] and Al_2O_3:C [3–9] are examples of phosphors spliced to the end of commercial silica and polymer fibres. The use of an intrinsic method, where the optical fibre itself produces the OSL effect, has been demonstrated using fluoride phosphate (FP) glass optical fibres [10, 11]. Although the

Optical Materials EXPRESS

concept of this type of dosimeter was demonstrated, the low sensitivity of the material limits the practical usage of these fibres as dosimeter devices. Thick fibres, canes, or bundles of fibres stacked together are necessary to achieve the required intensity to perform radiation-sensing measurements. Ideally, this sensor design should work with a single optical fibre, which requires enhancement of the OSL intensity from the glass. The work presented here demonstrates how this can be achieved with the addition of Tb^{3+} to the FP glasses.

Doping of glasses with rare earth elements has been extensively studied, but generally for the purposes of improving scintillation properties and not for OSL. Both mechanisms involve the creation of electron-hole pairs by ionising radiation, but unlike scintillation, during OSL this liberated charge becomes trapped at defect sites in the material, requiring optical stimulation to free it. However, for both scintillation and OSL recombination of electron-hole pairs may occur at dopant sites, this allows previous studies of scintillating materials to guide the fabrication of OSL-active glasses. Recent examples show increases in scintillation intensity due to rare earth ions in various materials: phosphate glass is shown to produce efficient scintillation with Tb^{3+} and Ce^{3+}-codoping [12], as is Tb^{3+}:Gd^{3+}-doped silicate oxifluoride glass [13, 14]. FP glasses co-doped with Ce^{3+} and Gd^{3+} have also intense scintillation [15]. Rare earth doped silica glasses are also common scintillation materials. Ce^{3+}-doped silica has been demonstrated as a highly efficient and rapid scintillation material [16–18], as have Yb^{2+} [19, 20] and Tb^{3+} [21] doped silica glasses.

In this paper doping with Tb^{3+} was used to enhance the OSL sensitivity of FP glass. Characterisation of the material using thermoluminescence (TL) and OSL showed various improvements to the structure of the electron traps, emission spectra and signal intensities. Optical fibres were fabricated from the material and used for dosimetry measurements under beta and X-ray irradiations. The Tb^{3+}-doped glasses and fibres showed improved performance compared with undoped glasses and fibres.

2. Glass and fibre fabrication

2.1. Glass fabrication

FP glass, obtained from Schott Glass Company, was used for the fabrication of Tb^{3+}-doped glasses and fibres. Doping with Tb^{3+} was performed using Tb_4O_7 in both oxidising and reducing atmospheric conditions, at a concentration of 1×10^{20} ions/cm^3. This concentration is comparable to concentrations used for previous studies of Tb^{3+} in FP glass, which used ion densities in the range of $0.1 - 10 \times 10^{20}$ ions/cm^3 [22, 23]. A concentration of 1×10^{20} ions/cm^3 was chosen as a compromise between enhancing the OSL properties of the glass and minimising optical fibre loss. Glasses made in 30 g batches were prepared for spectroscopy and OSL analysis, 100 g batches were prepared for optical fibre fabrication.

Glass melting in oxidising atmosphere Samples of FP glass were placed in a platinum crucible, the dopant compound was added and the crucible placed inside a furnace operating in ambient atmosphere. Samples were melted at 950, 1000 and 1050 °C for 1 to 3 hours. After dwelling in the furnace at temperature, samples were removed and swirled for approximately 20 s and then cast into a pre-heated brass mould. Following the cast, samples were allowed to cool before being placed into a separate furnace to anneal, where the temperature is increased to 450 °C and then cooled at a controlled rate of 0.1 °C/s. The sample was then removed from the mould and post-annealed at 450 °C to remove any residual stress in the glass. Initial melting trials were performed at 950 °C, but the glass was found to be too viscous for efficient casting, and a lot of glass remained in the crucible, therefore the temperature of remelts was raised to 1000 - 1050 °C for later experiments.

Optical Materials EXPRESS

Glass melting in reducing atmosphere Samples here were melted, cast and annealed within a glovebox with an attached furnace under a nitrogen atmosphere. Samples of FP glass were placed in a vitreous carbon crucible, the carbon crucible was cleaned prior to use by submersing in methanol, which was then placed in an ultrasonic bath for 15 minutes to remove any loose particles from the surface. The dopant compound was added and the crucible placed into the controlled atmosphere furnace, attached to the glovebox. Samples were heated to 900 °C and allowed to dwell for 1-3 hours. After sufficient dwell time, the glass was removed and swirled for approximately 20 s, then allowed to cool before being placed into a separate pre-heated furnace at 450 °C to anneal. Cooled samples were removed and post annealed at 450 °C in an ambient atmosphere to remove any residual stress in the glass.

Sample preparation The glasses from 30 g batches were cut into slides and polished for spectroscopy, samples were also crushed into 250 - 400 μm grains for TL and OSL analysis. Table 1 in Section 3.3 summarises the different samples studied here. The glasses from 100 g batches were cast into billets 30 mm in diameter and polished on all faces in preparation for extrusion into optical fibre preforms.

2.2. Fibre fabrication

Fibre fabrication was performed using the same method that has been reported previously for undoped FP glass fibres [24]. Due to the addition of Tb_4O_7 to the glass, a small change in the thermal properties of the glass was observed during fibre fabrication: undoped glasses required an extrusion temperature of 525 °C and a fibre drawing furnace temperature of 750 °C [24], whereas Tb^{3+}-doped glasses were found to require an extrusion temperature of 528 °C and a fibre drawing furnace temperature of 800 °C. The temperature values stated for fibre drawing are the furnace temperatures, not the temperature of the glass itself. The difference between the glass and the furnace temperature can differ by 200 - 300 °C [25].

All fibres were drawn as unclad and uncoated bare fibres, refractive indices for the Schott FP glass can be found from the supplier [26]. Fibre trial F1 was fabricated from undoped glass, as obtained from the supplier. Fibres from trial F2 were canes of 400 - 1000 μm diameter, made from reduced Tb^{3+}-doped FP glass, fibres from trial F3 were made from the same glass, but fabricated with diameters between 160 - 250 μm. Fibres from trial F4 were fabricated from oxidised Tb^{3+}-doped glass, with diameters between 160 - 250 μm. Loss of all fibres was measured using the standard cut-back technique [27], a comparison of the loss for fibres F1, F3 and F4 is shown in Fig. 1(b). Higher loss was measured in remelted fibres, potentially due to the addition of Tb^{3+} and/or remelting of the as-supplied glass. The higher loss of F3 could be due to scattering from graphite impurities, introduced from the crucible during melting.

3. Glass material characterisation

3.1. Spectroscopy

Absorption spectra were obtained using the Agilent Cary 5000 UV-Vis-NIR spectrophotometer from 200 to 1200 nm in transmission mode, losses due to Fresnel reflection are subtracted. For each slide, the thickness was measured in order to calculate and report absorption as loss in dB/m, results are shown in Fig. 1(a).

The Tb^{3+} $4f^8 \rightarrow 4f^7 5d$ transition at 215 nm, shown also in previous literature [22,23,28], shifts the UV absorption edge of the glass to a slightly longer wavelength and no transmission is seen at wavelengths below 230 nm. The absorption peaks observed between 300 and 400 nm are also described previously in the literature for Tb^{3+} doped fluoride phosphate glass [23]. Terbium in fluoride phosphate glass exists as Tb^{3+} for glasses remelted under both ambient and reducing

Optical Materials EXPRESS

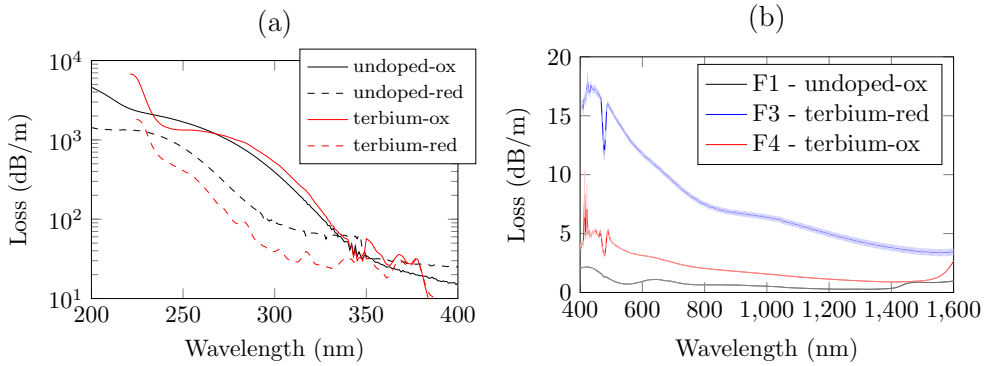

Fig. 1. (a) absorption spectra of fluoride phosphate glass samples: undoped (black) and Tb^{3+}-doped (red), melted under oxidising (solid) and reducing (dashed) atmospheres. (b) loss spectra of undoped and Tb^{3+}-doped fluoride phosphate optical fibres. Optical fibres were fabricated from glasses melted in both oxidising and reducing atmospheric conditions. F1: undoped-ox, F3: terbium-red, F4: terbium-ox. F2 was in the form of large-diameter canes, hence loss measurements were not performed.

atmospheres. Radiation exposure can cause the formation of Tb^{4+}, which has been previously shown to absorb at 370 nm [23], however, no significant peaks were observed here.

For both doped and undoped glasses, the absorption edge is shifted to shorter wavelengths in samples melted in reducing conditions. This is attributed to chemical reduction of metal ion impurities such as reduction of Fe^{3+} to Fe^{2+}. Fe^{3+} absorbs at 260 nm and Fe^{2+} absorbs at 220 nm [29], hence melting in a reducing atmosphere produces a greater proportion of reduced ions (Fe^{2+}) and the UV absorption edge is shifted to shorter wavelengths.

Emission spectra were obtained using 355 nm stimulation from a frequency-tripled YAG laser. The emission spectrum is shown in Fig. 2(a), emission peaks have been attributed to transitions based on a previous study of Tb^{3+} ions in fluoride phosphate glass [30].

The emission peaks of Tb^{3+} are a suitable match for the detection window of silicon avalanche photodiodes and the transmission window of Schott BG39 and Hoya U340 filters, shown in Fig. 2(b). The intense 550 nm emission peak from Tb^{3+} occurs at the highest quantum efficiency of the avalanche photodiode when optically filtered with a 3 mm thick Schott BG39 filter.

3.2. Thermoluminescence

The luminescence characteristics of undoped FP glass have been previously reported [31], and the luminescence analysis methods used here are similar to those used previously. In summary, most luminescence tests were performed using the Risø OSL/TL DA-20 Reader, which contains optical stimulation from LEDs at 470 nm and 870 nm and photon detection with an Electrontubes 9235QB bialkali photomultiplier tube. TL measurements were made using a heating rate of 1 K/s, and were performed between room temperature to 300 °C, reheat measurements were performed for each sample in order to subtract the incandescence from the heating plate observed at higher temperatures. TL emission spectroscopy was performed using the 3D-TL emission spectrometer, the method used for experiments is as described in [32]. Due to slight differences in thermal contact and heating efficiency, the TL peaks from TL emission spectroscopy are observed at slightly higher temperatures.

TL results are shown in Fig. 3(a) for both Tb^{3+}-doped and undoped samples prepared under both oxidising and reducing conditions. They demonstrate that Tb^{3+} doping produces an additional deeper electron trap in the material, shown by the occurrence of higher temperature TL

Optical Materials EXPRESS

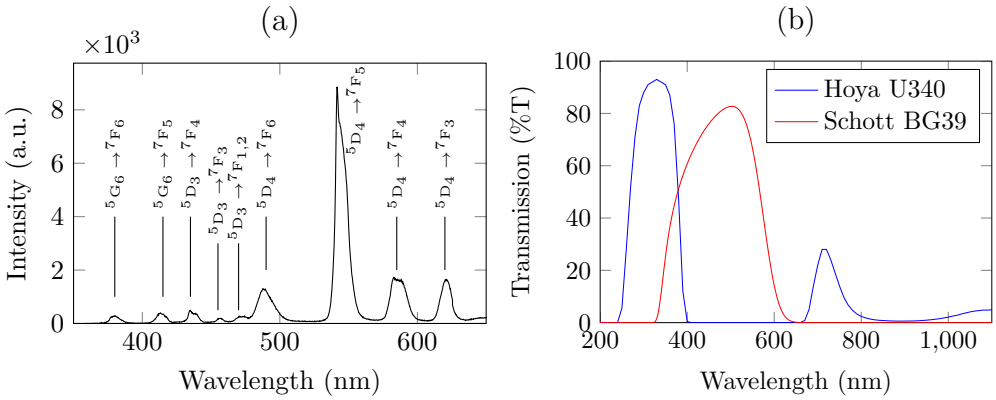

Fig. 2. (a) emission spectra of sample terbium-red. Excitation at 355 nm with frequency tripled YAG laser. Emission peaks are observed at suitable wavelengths for use with Schott BG39 and Hoya U340 filters. (b) Transmission spectra of the 7mm thick Hoya U340 and the 3 mm thick Schott BG39 coloured glass filters used for OSL measurements.

peaks in Fig. 3(a). Intense peaks were observed at 90 °C and 310 °C, the 90 °C peak obscures the 60 °C TL peak observed in undoped glass.

TL emission spectra are shown in Fig. 3(b). Several of the peaks observed in the optically-excited emission spectrum shown in Section 3.1 were observed, in particular the 550, 490, 440, 420 and 380 nm peaks. Due to the resolution of the instrument, the 440 and 420 nm peaks appear as one broad peak and the 590 peak also appears as a small shoulder on the 550 nm peak.

In order to obtain additional information on the trap depths, T_m, initial rise TL [33–35] was performed for terbium-red. The method used has been reported previously [31]. For TL occurring in the 300 °C region, lifetimes were calculated to be on the order of 10^{11} s. Traps at these higher energies are present in Tb^{3+}-doped samples but not in undoped samples, hence the lifetime of trapped electrons is significantly longer in Tb^{3+}-doped glass than for undoped glass. Where the population of trapped electrons in a sample of undoped glass might fade at room temperature after several minutes, the population of trapped electrons in a Tb^{3+}-doped sample may remain stable for hundreds to thousands of years.

3.3. *Optically stimulated luminescence*

OSL measurements were performed using the Risø OSL/TL DA-20 Reader in two different configurations: the first using 470 nm optical stimulation and a 7mm thick Hoya U340 filter placed before the PMT to block scattered stimulation light, the second using 870 nm optical stimulation and a 3 mm thick Schott BG39 filter. The transmission spectra for both these filters are provided in Fig. 2(b). All optical stimulations occurred for 5 s and the OSL intensity was integrated over the first 0.2 s of optical stimulation. Results were normalised for dosage and mass in order to account for any small variation in the amount of material between samples, results are therefore reported as counts/g/Gy.

Figure 4 and Table 1 compares OSL results for Tb^{3+}-doped samples prepared under both oxidising and reducing conditions with undoped samples. The most intense OSL response is produced by Tb^{3+}-doped glass prepared in oxidising conditions, measurements show it is approximately an order of magnitude more intense than all other samples.

Optical Materials EXPRESS

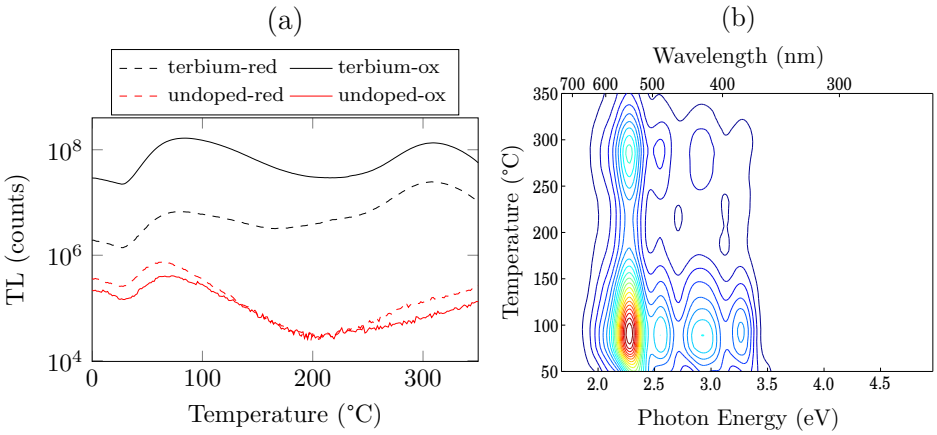

Fig. 3. (a) TL emission of undoped and Tb^{3+}-doped FP glass. (b) TL emission spectrum and intensity contour plot of sample terbium-red. The emission peaks observed previously are clearly visible in the 400 – 600 nm region.

Table 1. OSL response of doped and undoped FP glass, fabricated under both oxidising and reducing conditions, integrated from 0 - 0.2 s. 275 – 400 nm indicates OSL in this wavelength region, achieved using a HOYA U340 filter and 470 nm stimulation. 350 – 600 nm indicates emission in this wavelength region achieved with a Schott BG39 filter and 870 nm stimulation.

Sample	**Dopant**	**Redox**	**OSL (counts/g/Gy)** $\times 10^5$	
			275 – 400	**350 – 600**
undoped-ox	Undoped	Ox	75.6	8.8
undoped-red	Undoped	Red	107.3	12.3
terbium-ox	Terbium	Ox	1007.0	812.3
terbium-red	Terbium	Red	77.4	60.3

4. Radiation detection with optical fibres

4.1. *Experimental*

A diagram of the experimental setup is shown in Fig. 5, where optical stimulation and luminescence detection occur at the proximal end of the fibre. Optical alignment of the system is aided by a 532 nm guide laser coupled into the distal end of the fibre.

Irradiation sources A $^{90}Sr/^{90}Y$ foil source with an activity of 750 MBq was used for irradiation of fibres with beta particles having energies up to 2.28 MeV from the decay of ^{90}Y to ^{90}Zr. As the source has a face of 15 mm in diameter, only a short section of the total fibre length is therefore exposed for each test.

X-ray irradiation was produced using a Lorad LPX300 X-ray source. The filament current ranges from 0.1 - 10 mA; the tube voltage ranges from 10 - 300 kV, allowing variation of the photon energy spectrum produced. The maximum operating power is 900 W. Off the tungsten target, the X-rays are produced in an elliptical beam of 60° by 40°, allowing irradiation of the entire length of a fibre if it is coiled up within the beam.

Optical Materials EXPRESS

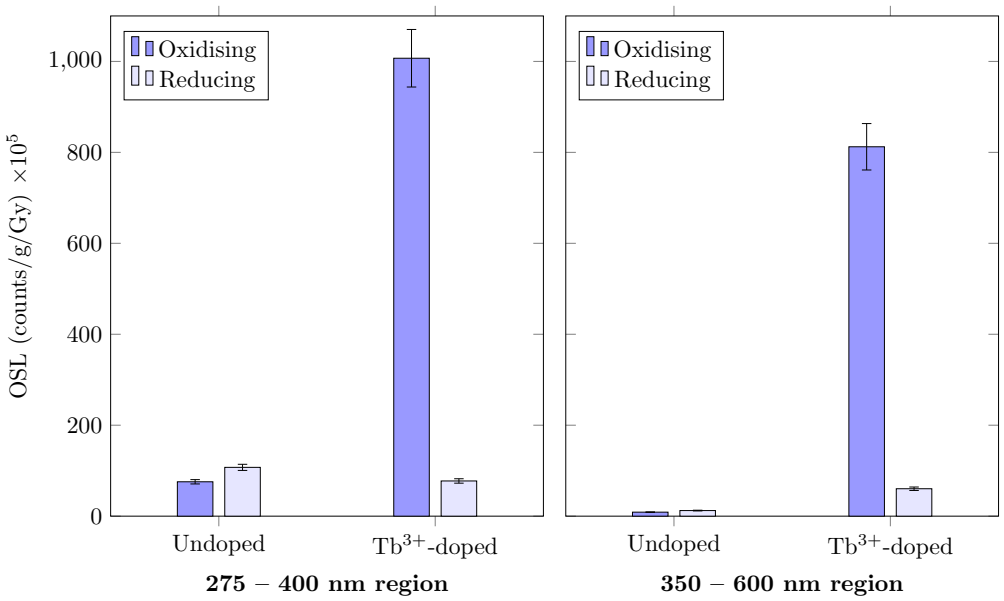

Fig. 4. Plot of the OSL data provided in Table 1, shown for both 275 – 400 and 350 – 600 nm wavelength regions. Results shown for samples fabricated under both oxidising and reducing conditions.

Fibre holders Optical fibres are mounted in an aluminium fibre holder for placement under the radiation source. Two holders are used, one in which fibres are coiled up beneath the source, and one in which the fibre rests unbent in a v-groove. The environment directly surrounding the optical fibre has an effect on the absorbed dose in the fibre, due mainly to bremsstrahlung X-rays generated in the fibre holder. In the case of the v-groove, the fibre is surrounded by aluminium beneath and to the sides, but is uncovered in the direction of the irradiation source; for the coiled fibre holder, the fibre is surrounded on all sides by aluminium.

Optical stimulation, signal filtering and detection Optical stimulation of the fibres was done using a 100 mW, 852 nm diode pumped laser, a Schott RG830 filter was used to attenuate the shoulder of the laser output. To filter scattered stimulation photons from the luminescence signal, the fibre output is passed through a 800 nm dichroic mirror and a 3 mm thick Schott BG39 filter. The transmission spectrum of the Schott BG39 filter is provided in Fig. 2(b), this can be compared with the emission spectrum shown in Fig. 2(a), indicating the suitability of matching the emission spectrum of Tb^{3+}-doped glass with the transmission of the BG39 filter. Luminescence counts are detected using a Lasercomponents COUNT10b single photon avalanche diode (SPAD), this detector is also isolated from the optical fibre and the stimulation laser by a light-tight housing.

Data collection Photon counting data is collected using an Ortec multichannel scaler, with a timing of 1 ms per channel. The data was then integrated from the onset of the OSL signal for 0.2 seconds, this value remained consistent for all measurements. A background was then established, while the optical stimulation was still active, by averaging over 1 second following depletion of the OSL signal; this background is then subtracted from the integrated OSL signal.

Optical alignment A 532 nm laser was coupled into the opposite end of the fibre to assist with optical alignment of the fibre output onto the SPAD. This light source was only used for setting

Optical Materials EXPRESS

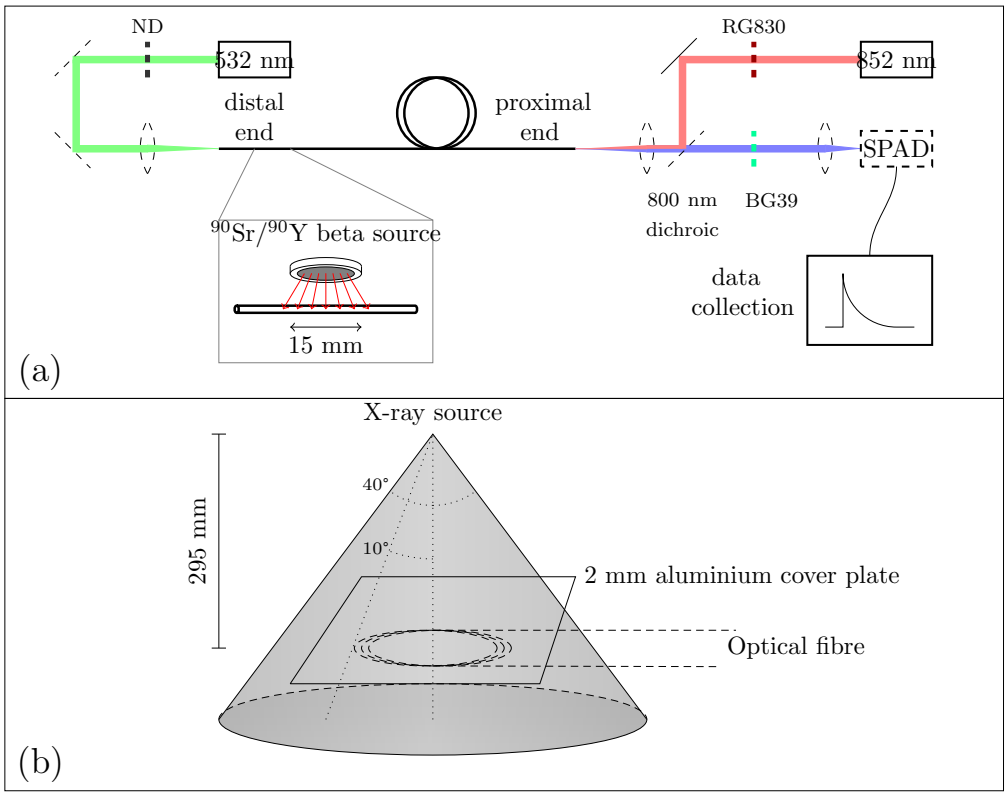

Fig. 5. (a) Experimental setup for the detection of OSL from a single optical fibre using a single photon avalanche diode (SPAD), irradiation is provided from a ^{90}Sr/^{90}Y foil source. 532 nm is used for optical alignment of the system, 852 nm is used for optical excitation during the OSL measurements. (b) Depiction of fibre irradiation when using the X-ray source, where the whole fibre is irradiated. All other parts of the experiment are identical to that shown in (a).

up each fibre experiment and had no role in the acquisition of OSL data.

4.2. *Beta irradiation*

OSL as a function of fibre size In previous work, OSL of undoped FP glass fibres was only reported for a bundle of fibres stacked together in order to improve the signal-to-noise [11]. To demonstrate improvement on this, a series of fibres were fabricated from terbium-red glass with varying diameters of between 160 and 1000 μm (Trials F2 and F3). OSL measurements were performed on each fibre with the ^{90}Sr/^{90}Y source located close to the proximal end of the fibre, a distance of 90 mm, to avoid excessive attenuation of the OSL signal. Fibres were irradiated for 120 seconds, which for fibres in the diameter range of 160 - 200 μm equates to a dose of 14.6 ± 0.5 Gy. Results shown in Fig. 6(a) indicate that an OSL signal is detected in the 160 and 200 μm diameter fibres, demonstrating single-fibre detection is possible.

OSL as a function of position along the fibre To demonstrate the functionality of an optical fibre based device as a distributed sensor, experiments were performed to measure the OSL response as a function of position along the fibre for fibres of several diameters. This experiment utilised Tb^{3+}-doped optical fibres fabricated from glass melted under oxidising conditions (Trial

Optical Materials EXPRESS

F4). OSL measurements were obtained with the ^{90}Sr/^{90}Y source at various positions along the length of the fibre, with a dosage of 14.6 ± 0.5 Gy (120 s irradiation time), results are shown in Fig. 6(b). The OSL intensities measured show that irradiations can still be detected a certain distance down the fibre, extrapolating the OSL intensity trend, detection using much longer lengths of fibre should be possible.

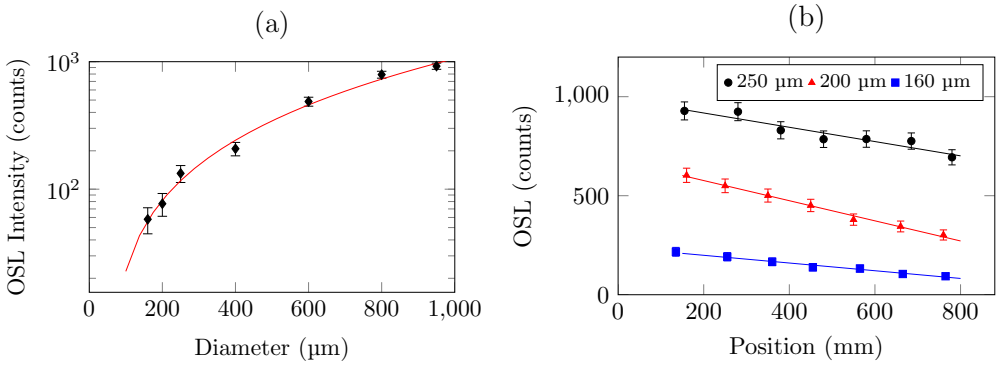

Fig. 6. OSL results of terbium-red fibres and canes using a dosage of 14.6 ± 0.5 Gy and detection in the 350 – 600 nm wavelength region using a Schott BG39 filter and approximately 20 mW of optical stimulation at 852 nm. (a) Intensity as a function of fibre diameter (950 – 400 µm were from fibre F2, and 250 – 160 µm were from fibre F3, both fibres from terbium-red). The trendline shows a quadratic fit. (b) OSL with respect to intensity as a function of the position of the ^{90}Sr/^{90}Y radiation source along fibre pieces from fibre F4 (terbium-ox), measured from the proximal end. Trendlines show a linear fit.

Maximum fibre length To further demonstrate the capability of the Tb^{3+}-doped fibres, the range down the fibre at which OSL measurements could still be performed was tested, again using fibre trial F4 (terbium-ox). The ^{90}Sr/^{90}Y source was placed at a distance down the fibre, and an irradiation of 14.6 ± 0.5 Gy was applied, after which an OSL measurement is taken. The distance along each length of fibre at which an OSL response was measured is reported in Table 2, along with the intensity measured. Also reported alongside each OSL measurement is the radioluminescence signal recorded prior to the OSL measurement.

As per Fig. 6(a), fibres with larger diameters have more intense OSL signals, due to the greater irradiated mass of material. However, optical alignment cannot be exactly replicated for each length of fibre tested, even when the careful alignment process is performed, cleave quality of thicker fibres was also more prone to variation. For this reason, thicker fibres frequently had a lower intensity OSL response than fibres with a smaller diameter, as can be seen in Table 2.

Results indicate successful OSL measurements using far longer lengths of optical fibre than has been previously reported for undoped FP glass optical fibres. An important point to highlight is the small irradiation area on the optical fibre, shown in Fig. 5, where only 15 mm of fibre receives a dose - a small fraction of the total fibre length. This demonstrates the localised sensing capability of these fibres, enabling point-sensing anywhere along its length. In addition, for applications where the radiation field is spread over a wider area, more fibre would become exposed and the OSL intensity proportionally higher for a given dose rate.

4.3. X-ray irradiation

OSL measurements were taken as a function of beam intensity at two different tube potentials, 100 and 300 kV. The beam intensity, in milliamp seconds (mAs), was changed by adjusting the

Optical Materials EXPRESS

Table 2. Distance along a Tb^{3+}-doped fibre of fibre trial F4 (terbium-ox) at which an OSL signal is measurable using an absorbed dose of 14.6 ± 0.5 Gy from a $^{90}Sr/^{90}Y$ beta source.

Fibre	Distance (m)	RL (counts/s)	OSL (counts)
160 μm	1.5	458 ± 21.4	148.5 ± 20.7
200 μm	2.6	164 ± 12.8	44.1 ± 13.0
250μm	2.4	221 ± 14.9	37.5 ± 12.9

filament current while using a constant exposure time of 60 s. Results can be seen in Fig. 7. The OSL intensity of fibre F4 (terbium-ox) is significantly more intense than fibre F3 (terbium-red), as is expected from the OSL results shown in Fig. 4.

For each X-ray tube potential and for each fibre, the OSL intensity is measured to increase with intensity due to the greater dose deposited in the fibres. But after a certain dosage, the effect of photodarkening in the fibres was observed to reduce the measured OSL intensity, due to a radiation-induced increase in the fibre loss. Since detection is occurring in the 300 – 600 nm transmission window of the Schott BG39 filter, photodarkening is attributed to phosphorous-oxide hole centres (POHC) which occurs as a broad peak centred at 450 nm [36, 37]. The onset of photodarkening is observed to occur at a higher dose in fibre F3 (terbium-red) than fibre F4 (terbium-ox). Compared to F4, in the fibre F3 made from glass melted under reducing conditions the metals ions are present in the lower valence state, which makes them act as additional hole traps. The formation of metal ion based hole centres, which absorb in the UV [23], i.e. not within the 300-600nm detection window, competes with the POHC formation. Consequently, for the F3 fibre, the POHC formation requires higher dose and thus photodarkening in the 300-600nm detection window occurs at higher dose.

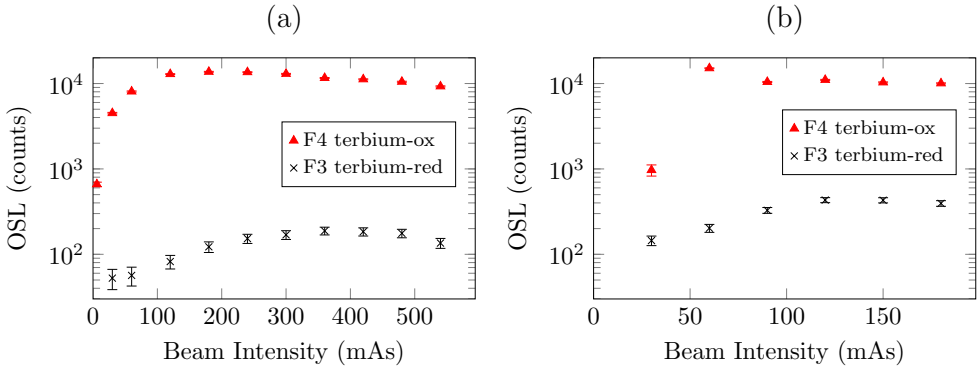

Fig. 7. OSL results following X-ray irradiation of 200 μm fibres from trials F3 (terbium-red) and F4 (terbium-ox). Irradiations were performed over a range of X-ray beam intensities, using X-ray tube potentials of (a) 100 kV and (b) 300 kV.

5. Conclusions

Fluoride phosphate glasses doped with Tb^{3+} ions were shown to have improved OSL intensity compared to undoped fluoride phosphate glass. An OSL response of 812.3×10^5 cnts/g/Gy for oxidised Tb^{3+}-doped glass was measured, compared with 8.8×10^5 cnts/g/Gy for undoped oxidised FP glass samples in the 350 - 600 nm region. Tb^{3+}-doped glasses fabricated in an oxidising atmosphere were also shown to have a more intense OSL response than glasses fabricated in reducing atmosphere, the OSL response of 812.3×10^5 cnts/g/Gy for oxidised

Optical Materials EXPRESS

Tb^{3+}-doped glass is compared with a value of 60.3×10^5 cnts/g/Gy for reduced Tb^{3+}-doped FP glass samples in the 350 - 600 nm region.

This increase in OSL intensity is attributed to the recombination of electron-hole pairs occurring in the Tb^{3+} ions, producing emission in the wavelength region suitable for optical filtering with a Schott BG39 filter and detection with a SPAD. The addition of Tb^{3+} might also produce additional electron/hole traps, allowing a larger amount of charge to remain trapped in an excited state following irradiation. The cause of higher OSL intensity from the oxidised Tb^{3+} doped glass with respect to the reduced Tb^{3+} doped glass is currently unknown.

Optical fibres were fabricated from Tb^{3+}-doped fluoride phosphate glass and tested under beta and X-ray irradiation. For fibres fabricated from terbium-ox, at distance of 2.6 m along the fibre 44.1 ± 13.0 counts were measured following a dose of 14.6 ± 0.5 Gy from a $^{90}Sr/^{90}Y$ beta source. For undoped optical fibres, a detectable OSL result was only measurable using a bundle of fibres at a distance of 0.09 m from the fibre output [11]. These results indicate optical fibres can be used for distributed radiation sensing applications using the OSL mechanism. An event occurring anywhere along the length of the fibre will be detected, enabling monitoring over a wide area. Furthermore, any dose from a large radiation field covering a longer length of the fibre will be integrated along its length, increasing sensitivity.

Optical fibres might be further improved by optimising the fabrication conditions to reduce the loss, this may be a product of either glass remelting or due to the addition of Tb^{3+}. The optimum concentration of Tb^{3+} should also be further investigated to optimise the OSL intensity.

Funding

Defence Science and Technology Group;
The Optofab node of the Australian National Fabrication Facility utilizing Commonwealth and South Australian State Government funding;
Australian Research Council Research Hub for Australian Copper-Uranium

Acknowledgements

Alastair Dowler is acknowledged for technical assistance with drawing of optical fibres.